

Porous carbon nanofiber monolith binder-free derived from stink bean pod peel as electrode material for symmetric supercapacitor application

E. Taer^{a*}, A. Apriwandi^a, Z. Purba^a, R. Taslim^b

^a*Department of Physics, Faculty of Mathematics and Natural Sciences, University of Riau, 28293 Simpang Baru, Riau, Indonesia*

^b*Department of Industrial Engineering, State Islamic University of Sultan Syarif Kasim, 28293 Simpang Baru, Riau, Indonesia*

Activated carbon bio-wastes-based have been extensively studied as electrode material for symmetric supercapacitor. In this work, the activated carbon stink bean pod peel-based was synthesis with simplest possible technique without involving complicated techniques as electrode material for supercapacitor. Stinky bean pod peel-based activated carbon is prepared through pre-carbonization, chemical activation, carbonization, and physical activation. $ZnCl_2$ in four different concentrations of 0.1, 0.3, and 0.5 $m L^{-1}$ was selected as chemical reagent. Furthermore, the carbonization and physical activated were performed in furnace tube in high temperature. The physical features obtained indicate the potential of stink bean pod peel as activated carbon with a nanofiber structure and decorated by rod-like structure. In symmetric supercapacitor, the capacitive behavior was obtained as high as 265 $F g^{-1}$ in 1 M H_2SO_4 aqueous electrolyte. In addition, the maximum energy density was found of 36.18 $Wh kg^{-1}$ with power density of 125.06 $W kg^{-1}$. This simple method of obtaining activated carbon from stink bean pod peel provides a perspective for the further development of high-performance electrode materials for supercapacitor applications.

(Received June 29, 2021; Accepted October 15, 2021)

Keywords: Activated carbon, Nanofiber, Stink bean pod, Electrode material, Supercapacitor

1. Introduction

Stink bean (*Parkia speciosa*) is a tropical legume tree in the Leguminosae family that is popular from Southeast Asia, especially Indonesia which has a characteristic odor but is usually consumed in a variety of cooked local dishes. Stink beans are commercially available in traditional markets almost all year round throughout Indonesia. On the other hand, stink bean contains various bioactive compounds which have strong beneficial functions, for example, antifungal activity, antidiabetic and antihypertensive potential [1,2]. In order to meet this need, the production of stink beans is increasing every year. As an agricultural crop, the increase in stink bean production is of course followed by organic waste as part of the by-products of Indonesian people's consumption, especially their stink bean pod peel. This organic waste is usually a household waste problem and is left to decompose without further utilization, while the potential for this organic waste is quite promising to be processed and made into high-value products such as activated carbon sources for absorbents [3], water purification [4], and even as electrode material for energy storage application [5].

Activated carbon (AC) is a porous material that has a high specific surface area and an adjustable and suitable pore structure greatly contributes to the adsorption capacity [6]. Thus, wider applications can be attributed to such properties as adsorbents, water-air purification, and energy storage such as lithium-ion batteries, fuel cells, and supercapacitors [7]. However, the high cost of preparation and the fabrication process that requires complex techniques are a big challenge for increasing use and greater application. This important issue has given rise to continuous research and found that organic waste has the potential to be used as a source of activated carbon [8]. This is due to the activated carbon source from organic waste or bio-waste is

* Corresponding author: erman.taer@lecturer.unri.ac.id

abundant, never exhausted, renewable, cheaper, affordable, and easier to fabricate without the need for complex technique arrangements [9,10]. On this note, activated carbon has been investigated a lot as a raw material for electrodes as energy storage, especially supercapacitors [11,12]. Some of the by-products of agricultural plants as activated carbon for supercapacitor electrodes include jengkol shell [13], durian shell, mangosteen peel [14], banana peel, and pineapple leaf [15]. They performed excellent results as supercapacitor electrode devices with high surface area and outstanding specific capacitance.

Recently, the porous carbon material from garlic peel [16] and banana leaves [17] has confirmed ultra-high surface area from 1469 to 3325.2 m² g⁻¹ which can increase the specific capacitance from 190 to 424.42 Fg⁻¹ in the two electrode systems. Similar results were also confirmed by Selvaraj *et al.*, 2021 who have produced ultrahigh specific capacitance from materials from *Prosopis Juliflora* wood for supercapacitor applications [18]. Although they have described a preparation technique that is simple, relatively low-cost, and easily controllable, they still use a powder form with adhesive material including PVP/PVDF/PTFE for the supercapacitor cell assay system thus reduce the real conductivity of the raw material and increase the internal resistance. In addition, their energy density is considered to be relatively low which is not balanced with high power density thus limiting further applications. Furthermore, the electrolyte used is classified as a synthetic material and is not environmentally friendly.

The performance of nanofibers is continually improved through their physicochemical properties, structure, and texture. This is achieved through several synthesis methods including chemical vapor deposition [19], template [20], thermal-phase separation [21], and electrospinning [22,23], which is mostly used to obtain high nanofiber. The method is cost-effective, flexible, and can control high nanofiber structures [4]. Furthermore, it converts fibers into relatively dense arranged yarns by spinning Polyacrylonitrile (PAN) polymer material. It can also provide relatively high porosity, surface area, presence of hetero-atoms, and high conductivity to enhance the electrochemical properties of supercapacitors [22,23]. Several previous reports have synthesized carbon nanofibers through electrospinning techniques. It was reported that the method improved specific capacitance from 90 F g⁻¹ to 200 F g⁻¹ [22]. Meanwhile, Wang *et al* 2021 reported that carbon nanofiber having a surface area of 1468 m² g⁻¹ with micro-mesopores structure through the polymer blend of PAN/PANI and Novolac (NOC) produced specific capacitance as high as 394 F g⁻¹ [24]. Similar results were also reported by Xu *et al.* 2018 [25] and Lu *et al.* 2019 [26]. However, the electrospinning method has several limitations such as requiring special instruments with high voltage power, relatively low production rates due to toxicity from using polymeric materials, difficulty to obtain 3D formation, and non-adjustable pore diameter. In addition, the concentration, viscosity, humidity, pressure, temperature, surface tension, and the solvent of the polymer material used should also be considered.

In this study, the stink bean pod peel (SBP) was used as the raw material for activated carbon nanofiber as the electrode for supercapacitor applications. The stink bean pod peel conversion process was prepared by the simplest possible method without involving complicated techniques. Activated carbon was obtained through the ZnCl₂ impregnation process and continued with the carbonization process and physical activation in one stage of pyrolysis in the N₂ and CO₂ gas environment. For the record, activated carbon is made in the form of solid pellets without added the adhesive synthetic materials. This is due to maintaining the real conductivity of the electrode material. Furthermore, the physical properties obtained indicate the potential of stink bean pod peel as activated carbon with a nanofiber structure. Based on the two-electrode configuration, the specific capacitance that has been obtained is 265 F g⁻¹ in a 1 M H₂SO₄ electrolyte. These results confirm that the bio-waste of stink bean pod peel can be considered as one of the raw materials for activated carbon with a nanofiber structure for electrode material as an electrochemical energy storage application.

2. Experimental

2.1. Synthesis of activated carbon nanofiber

Stinky bean pod peel-based activated carbon is prepared through a simple and facile method consisting of a series of pre-carbonization, chemical activation, carbonization, and physical activation. Stinky bean pod peel waste is obtained from the main market of Pekanbaru City. Next, the samples are cleaned, sundried, and cut into small pieces with a size of $\pm 1 \times 2$ cm. Stinky bean pod peel samples were pre-carbonized in an oven vacuum at 250 °C for 2.5 hours. Chemical activation was carried out by mixing carbon with ZnCl_2 in varying molarity ratios including 0.1 M, 0.3 M, 0.5 M, and 0.7 M, respectively. The obtained sample powder was converted into 20 pellets without the addition of adhesive synthetic materials. Furthermore, the carbonization and physical activation processes are performed in one step pyrolysis at N_2 - CO_2 gas environment in furnace tube. The pyrolysis process begins with the carbonization from standard temperatures to 600 °C in an N_2 gas environment and it was continued with physical activation in a CO_2 gas environment up to a maximum temperature of 850 °C. Finally, the sample was neutralized using DI water.

2.2. Characterizations

Stinky bean pod peel-based activated carbons are characterized by their physical and electrochemical properties including density calculations, microstructure, surface morphology, chemical elemental composition, specific capacitance, energy, and power, respectively. Density was evaluated based on the dimensions of carbon pellets including mass, thickness, and diameter [27]. X-ray diffraction (XRD) method was used to examine the microstructure of carbon samples with $\text{CuK}\alpha$ as a source. The space interlayer of d_{002} - d_{100} is determined based on the Bragg's equation and the layer height/layer width (L_c/L_a) is calculated using the debye-scherer equation [28]. Furthermore, the surface morphology and chemical composition were reviewed using scanning electron microscopy (SEM) and energy dispersive spectroscopy (EDS) methods through the JEOL-JSM360LA instrument. The electrochemical properties of supercapacitors including specific capacitance, energy, and power were determined by two different methods including cyclic voltammetry (CV) and galvanostatic charge-discharge (GCD) in the form of a sandwich which consists of two electrodes, an organic separator, and 1 M H_2SO_4 as electrolyte. In addition, these values are calculated using standard equations [29,30].

3. Results and Discussions

3.1. Materials features analysis

In the form of monolith without adhesive material, changes in the density of the activated carbon are considered necessary to be evaluated. The pyrolysis process and physical activation greatly affect the density of the carbon monolith, including the 0.1SBP, 0.3SBP, and 0.5SBP samples. The pyrolysis process is needed to convert the precursor sample into fixed carbon through evaporation of volatile compounds, water content, and nutrients [31,32]. In addition, this has a major impact in degrading lignocellulose so as to optimize the unique structure of the material from biomass. This process significantly affects the density of the carbon monolith sample. As shown in Figure 1, the three chemically immigrated samples showed density shrinkage after the pyrolysis process with values of 0.56, 0.70, and 0.58 g cm^{-3} , respectively. Pyrolysis which performed from 30 to 600 °C in detail can completely evaporate the volatiles and water content [33]. Furthermore, lignocellulosic compounds including hemicellulose, cellulose, and lignin gradually decompose [34]. Hemicellulose decomposes at a temperature range of 150 to 240 °C, followed by cellulose from a temperature of 250 to 350 °C [35]. Lignin is the component that decomposes the longest at a temperature of 160 to 900 °C [36]. Furthermore, ZnCl_2 impregnation begins to react with carbon at temperatures above 500 °C [37]. This reaction produces oxidative compounds that erode the carbon matrix framework. These processes significantly alter and degrade the dimensions of SBP carbon monoliths in particular mass, thickness, and diameter so that their density is significantly reduced. Moreover, physical activation using CO_2 gas in the

temperature range of 600 to 850 °C allows the expansion of the carbon matrix and opens the possibility of more pores large so that the porosity increases drastically [38]. Finally, the decrease in carbon monolith density of SBP was 40.42%, 20.45%, and 32.56% for samples 0.1SBP, 0.3SBP, and 0.5SBP, respectively.

The SBP activated carbons that have been obtained are reviewed for their microstructural properties through the X-ray diffraction (XRD) technique. Figure 2 shows the XRD pattern for activated carbon based on stink bean pod peel waste at concentrations of 0.1 M and 0.5 M ZnCl₂, respectively. Based on this XRD pattern, the samples consistently showed two broad peaks at 2θ angles 24° and 44° which correlated with the scattering planes of 002 and 100. This is indicated that the samples obtained are carbon with an amorphous structure [39,40].

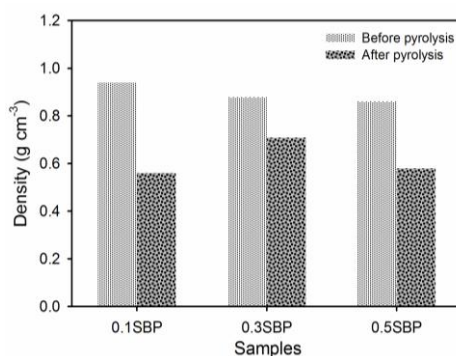


Fig. 1. Average density before and after pyrolysis of all samples.

Furthermore, an increase in the concentration of ZnCl₂ from 0.1 M to 0.5 M indicates a larger shift of the peak width as found in the 002 scattering plane from 24.20° to 24.98° and the 100 scattering field from 43.34° to 44.76°. This is due to the more ZnCl₂ impregnation at 0.5 M allows the reaction of carbon with the chemical reagent to produce co-product ZnOCl and evaporate more impurities thus that various pores begin to form and spread irregularly on the surface of the sample [41,42]. This property significantly contributes to increasing the contact area of the ion and electrode thereby increasing the electrochemical parameters of the supercapacitor. This analysis is in agreement with several previous studies [43,44]. In addition, the XRD pattern in Figure 2 also shows the presence of sharp peaks at 2θ angles of 39° and 42° indicating that relatively small amounts of crystalline compounds were found in the sample. These compounds can be CaCO₃ and MgO [45] as confirmed in the elemental analysis discussed below. In addition, d_{002} and d_{100} were evaluated using Bragg's law and have values of 3.94-398 Å, and 2.02-2.06 Å, respectively. This is a relatively normal value for biomass-based amorphous carbon [28,46]. Furthermore, L_c/L_a was determined through the Debye Scherer equation with values of 2.34 and 4.97 for 0.1 M and 0.5 M samples, respectively. These values can be used to predict the surface area of the samples as discussed previously. Based on the empirical formula, the smaller L_c/L_a ratio is indicated to have the highest surface area and this is very advantageous to improve the performance of supercapacitor electrodes.

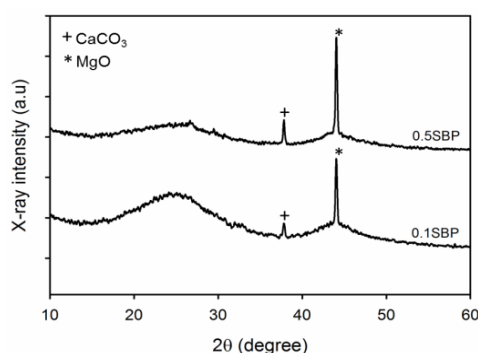


Fig. 2. XRD pattern of 0.1SBP and 0.5SBP samples.

The morphological structure of activated carbon stink bean pod peel-based for 0.1 M and 0.5 M samples is illustrated in Figure 3. The 0.1 M ZnCl_2 impregnation sample showed a structure morphology consisting of large lumps and aggregations at a range size of 1.32-2.29 μm with a flat and smooth surface (Figure 3a). In addition, in the selected magnification area, sample 0.1 M showed a morphological structure resembling a rod-like with a diameter of about 60-75nm. This result is almost similar to some activated carbon from other waste biomass such as cassava petiole, etc. [47,48]. Furthermore, the activated carbon sample impregnated with 0.5 M ZnCl_2 showed different surface morphology (Figure 3b). The addition of a concentration of ZnCl_2 greater than 0.1 M can extract the constituent components of biomass such as cellulose, hemicellulose, and lignin. ZnCl_2 reacts with the raw material at high temperatures to evaporate the volatiles and hemicellulose and release lignin in the cellulose. The cellulose is then eroded by heat thus exhibited nanofibers structure in various sizes. In the large magnification area, the 0.5 M sample reviewed a nanofiber structure with a diameter size range of 71-125nm. The nanofiber structure in the sample is considered to have the potential to improve the performance of the supercapacitor. This is due to high conductivity, providing varying pore sizes from micro and mesoporous and producing high surface area [49,50]. These advantages can consistently increase the specific energy and maintain the high specific power of the supercapacitor energy storage device [22,51]. As a comparison, these results are similar to other waste-based activated carbons that can improve the performance of supercapacitors such as pineapple leaves [52], bacterial-cellulose [53], and Pinewood [54]

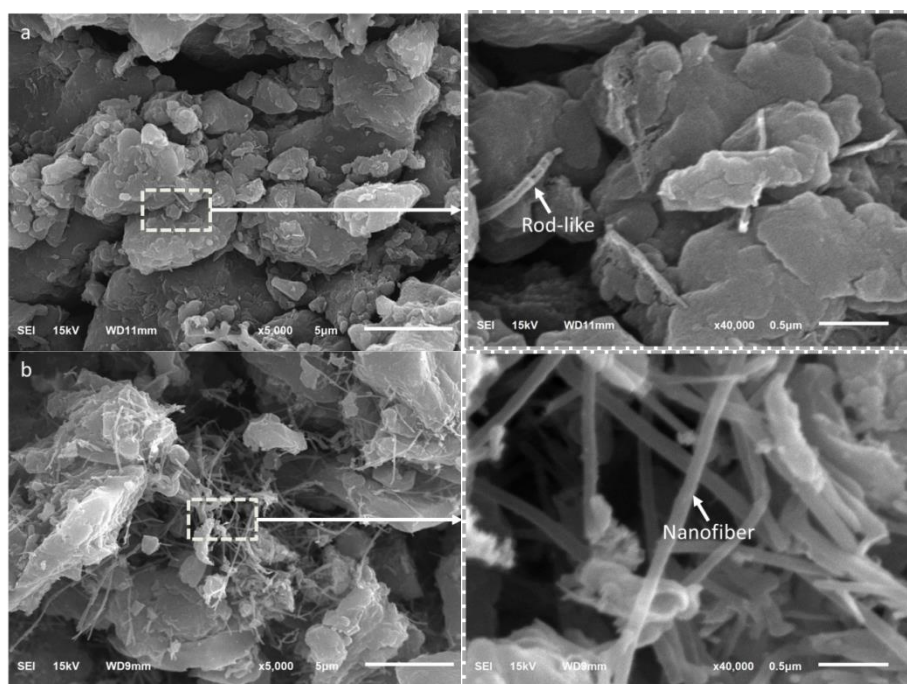


Fig. 3. SEM micrograph of 0.1SBP and 0.5SBP samples.

Elemental analysis of 0.1SBP and 0.5SBP ZnCl_2 impregnated activated carbon was reviewed through energy dispersive spectroscopy techniques, as summarized in Table 1. Elemental carbon (C) predominated for both samples with values of around 93-95%, followed by oxygen (O) of 4-5%, magnesium (Mg) of 0.13-0.22%, aluminum (Al) of 0.01-0.11%, silicon (Si) of 0.06-0.10%, and (K) of 0.07-0.14%. In fact, the 0.1 M ZnCl_2 impregnated sample had the highest carbon content while increasing the ZnCl_2 concentration up to 0.5 M could reduce the carbon content to 93.94%. This is probably due to the large amount of impregnated ZnCl_2 causing high oxidative formation which confirmed by the increased oxygen content of the 0.5 M sample. Furthermore, this high elemental oxygen can be attributed to its pseudo-capacitance because it can act as self-doping in the electrode material [55,56]. This feature can also improve the performance

of supercapacitor electrodes. This analysis is of course followed by CV and GCD profiles in Figures 4 and 6. In addition, the appearance of impurities in small amounts such as magnesium 0.13-0.22%, aluminum 0.01-0.11%, silicon 0.06-0.10%, and potassium 0.07 -0.14% contributed by the basic constituents of bio-waste, especially stink bean pod peel waste.

Table 1. The elemental analysis of SBP porous carbon nanofiber.

Samples	Element analysis					
	C (%)	O (%)	Mg (%)	Al (%)	Si (%)	K (%)
0.1SBP	95.46	4.23	0.13	0.01	0.10	0.07
0.5SBP	93.94	5.53	0.22	0.11	0.06	0.14

3.2. Electrochemical behaviours analysis

The electrochemical properties of SBP activated carbon nanofiber was thoroughly evaluated including specific capacitance, specific energy, specific power, and internal resistance through cyclic voltammetry and galvanostatic charge-discharge techniques. The supercapacitor cell was prepared in a solid monolithic two-electrode system without an adhesive. H_2SO_4 was selected as the electrolyte in a concentration of 1M and the organic separator was derived from duck eggshell membrane. As shown in Figure 4, the CV profile shows a slightly disturbed quasi-rectangular shape for all three SBP samples confirming the normal electrochemical double-layer capacitor feature [57]. More specifically, 0.1SBP actually displays a nearly perfect rectangular hysteresis loop curve indicating relatively good EDLC properties without heteroatom interference and contamination [58]. This is due to the high carbon content (as confirmed by EDS) allows the formation of a suitable matrix framework without other elemental contamination for ions to diffuse on the electrode surface. Furthermore, the addition of chemical activation concentration in 0.3SBP and 0.5SBP samples showed relatively different CV profiles.

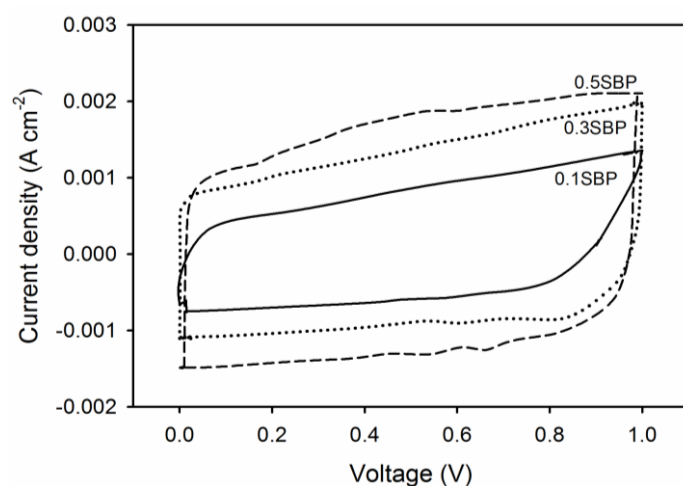


Fig. 4. Cyclic profiles of the symmetric supercapacitor.

The rectangular hysteresis loop curve begins to distort at a certain voltage range, both in the charging process and in the discharge process. This disturbance was seen more clearly in the 0.5SBP sample. At the time of charging, the current surge occurs in the voltage range of 0.2-0.5 V while in the discharge process it is found in the voltage range of 0.8-0.6V. This indicates the presence of pseudo-capacitance behavior in addition to the dominant EDLC properties [59,60]. This is due to the presence of heteroatoms that act as doping leading to faradaic redox reactions. Oxygen is thought to be the heteroatom that produces this property, as reported in a recent study [61,62]. As shown in Table 1, chemical impregnation at high concentrations can increase

elemental oxygen, especially in the 0.5SBP sample up to 5.53%. High oxygen content is clearly self-doping for electrode materials, especially those from biomass. The combination of these properties of EDLC and pseudo-capacitance can improve the performance of electrode materials for energy storage devices. Based on the standard equation, the specific capacitance obtained from each chemically activated sample with concentrations of 0.1, 0.3, and 0.5 M was 185, 202, and 264 F g^{-1} , respectively. Chemical impregnation at high concentrations can significantly boost the capacitive properties of supercapacitor cells. From a concentration of 0.1 M to 0.5 M of ZnCl_2 , the capacitance can be increased almost twofold. This is due to the chemical impregnation of 0.5M ZnCl_2 at high-temperature pyrolysis can optimize the morphological structure of the sample with dominated by nanofibers at a relatively small diameter of 71-125nm, as confirmed in SEM micrographs. This facilitates the formation of a carbon pore matrix at the micropores and mesopores scales providing a high diffusion field and relatively unimpeded ion immigration pathway [53,63]. In addition, the increased oxygen content also contributes to the wettability properties so that the capacitive properties are maximized [64].

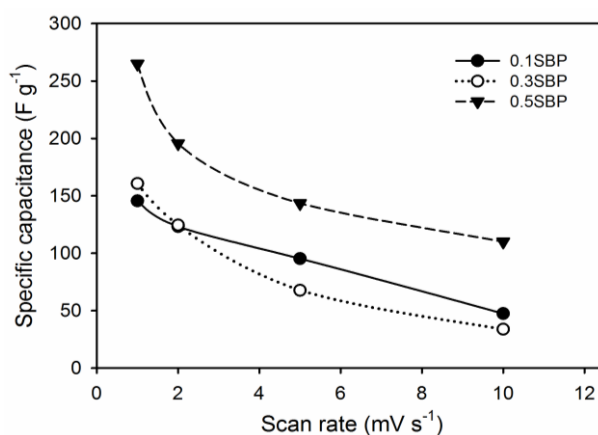


Fig. 5. The specific capacitance in different scan rate

Furthermore, different scan rates were also applied to the supercapacitor symmetric cells as shown in Figure 5. The increase in scanning rate also affects the symmetric capacitive properties of the supercapacitor, as shown in Figure 5. However, Sample 0.5SBP still maintained high capacitive properties at 5 mVs^{-1} scan rate of 119 Fg^{-1} , while 0.1SBP and 0.3SBP only maintained specific capacitances of about 56% and 61%, respectively. This is closely related to the morphological structure and framework of the carbon pore matrix formed.

An in-depth evaluation of the electrochemical properties was further confirmed through the galvanostatic charge-discharge technique. Samples 0.1SBP, 0.3SBP, and 0.5SBP displayed an isosceles triangular GCD profile at a constant current density of 1.0 A g^{-1} , as shown in Figure 6. This confirmed the normal porous carbon-based EDLC properties for electrochemical energy storage devices. The 0.1SBP sample displays charge times that are relatively equivalent to discharging times indicating ideal EDLC properties. Furthermore, the 0.3SBP and 0.5SBP samples confirmed their relatively longer charge times compared to their discharge times, thus displayed a relatively perturbed triangle. This clearly confirms the pseudo-capacitance feature of the symmetric supercapacitor, which is in agreement with the CV analysis discussed previously. The second highest oxygen content gives wettability properties so that it causes a faradaic redox reaction in the electrode material. Furthermore, the specific capacitances obtained were 168, 190, and 265 F g^{-1} for samples 0.1SBP, 0.3SBP, and 0.5SBP, respectively. Chemical impregnation using ZnCl_2 resulted in a specific capacitance that increased as the applied concentration increased. ZnCl_2 at higher concentrations can open the carbon matrix framework on the basic components of biomass and rearrange it to produce nanostructures [65], especially nanofibers. The dominant nanofiber structure on the sample surface causes the formation of controlled pores, especially in the micropores and mesopores ranges, and exhibits high electrical conductivity [66].

Furthermore, ZnOCl as a co-product of the first reaction ZnCl_2 and carbon facilitates the formation of oxidants and high oxygen content in the sample. This is closely related to the heteroatom self-doping effect that gives rise to the pseudo-capacitance property. In addition, the iR drop was not found clearly in the GCD profile for all samples, indicating that the symmetric internal resistance of the supercapacitor is relatively very low with values of 19, 11, and 8 $\text{m}\Omega$ for the 0.1SBP, 0.3SBP, and 0.5SBP samples, respectively.

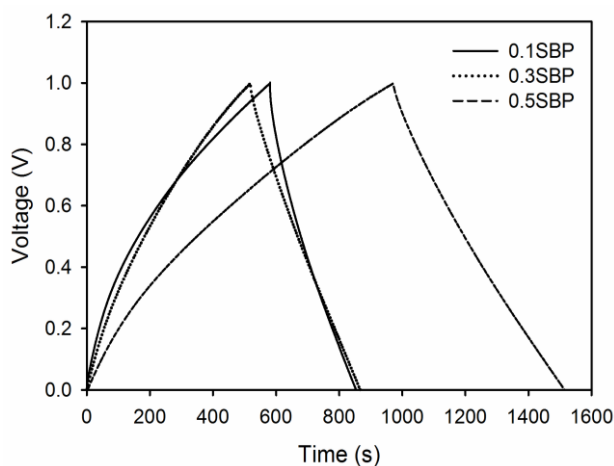


Fig. 6. The GCD profile of symmetric supercapacitor cell derived from SBP porous carbon nanofiber.

The energy density and power density of the carbon nanofiber-based symmetric supercapacitor are also reviewed in detail, as shown in Figure 7. The highest energy density and power density were found in the 0.5SBP sample with maximum values of 36.18 Whkg^{-1} and 125.06 Wkg^{-1} , followed by samples 0.3SBP and 0.1SBP with a maximum energy of 18.8534 and $10.4169 \text{ Whkg}^{-1}$ at a maximum power density of 110.22 and 87.98 Wkg^{-1} , respectively (in detail as shown in Table 2). The maximum energy density and maximum power density of carbon nanofibers exhibited in this study were higher than other studies using bacterial cellulose for carbon nanofibers with an energy density of 6.9 Wh kg^{-1} with a power density of 128.3 W kg^{-1} in aqueous electrolytes [53].

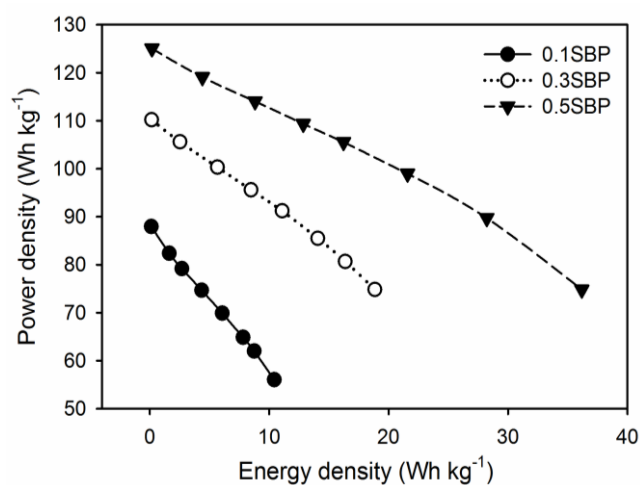


Fig. 7. Ragone plot of symmetric supercapacitor cell based on SBP porous carbon nanofiber

Table 2. The electrochemical features of the SBP symmetric supercapacitor cell based on CV and GCD techniques.

Samples	CV			GCD			
	C_{sp} (F g ⁻¹)	E (Wh kg ⁻¹)	P (W kg ⁻¹)	C_{sp} (F g ⁻¹)	E (Wh kg ⁻¹)	P (W kg ⁻¹)	R (mΩ)
0.1SBP	185	25.78	92.90	168	10.41	87.98	19
0.3SBP	202	28.15	101.44	190	18.85	110.22	11
0.5SBP	264	36.79	132.57	265	36.18	125.06	8

4. Conclusions

In summary, the activated carbon bio-waste stink bean pod peel-based with simplest possible method was successfully fabricated for electrode material as energy storage application of supercapacitor. The activated carbon was prepared by using ZnCl₂ impregnation in different ratio molarity and followed by carbonization and physical activation at N₂-CO₂ gas atmosphere. Overall, the activated carbon obtained showed relatively normal amorphous properties. Furthermore, the addition of ZnCl₂ molarity to the precursor can significantly change the activated carbon structure from a rod-like structure to a nanofiber structure with a diameter range of 71-125nm. In addition, carbon content occupies the most dominant element in all samples with a percentage of 93.94-95.46% and followed by oxygen of 4.23-5.53%. The electrochemical properties of the supercapacitor were tested in a two-electrode system with a specific capacitance of 265 at a constant current density of 1.0 A g⁻¹. In addition, the sample can maintain a capacitance of 68% at a scan rate of 10 mV s⁻¹. Finally, this simple method can provide activated carbon with a nanofiber structure from stink bean pod peel and can also be extended in energy storage and conversion.

Acknowledgments

The research was financially supported by *Kementerian Pendidikan, Kebudayaan, Riset, dan Teknologi*, Republic of Indonesia through third years Project of *Penelitian Dasar* (PD), contract No. 1418/UN.19.5.1.3/PT.01.03/2021 with the title “High-density micro-and nano carbon fiber made from biomass based materials for supercapacitor electrodes”.

References

- [1] I. I. Misnon, N. K. M. Zain, T. S. Lei, B. L. Vijayan, R. Jose, *Ionics* **26**, 4081 (2020).
- [2] Y. Asikin, Kusumiyati, T. Shikanai, K. Wada, *J. Adv. Res.* **9**, 79 (2018).
- [3] T. Qiu, J. G. Yang, X. J. Bai, Y. L. Wang, *RSC Adv.* **9**, 12737 (2019).
- [4] S. Soltani, N. Khanian, T. S. Y. Choong, U. Rashid, *New J. Chem.* **44**, 9581 (2020).
- [5] A. A. Mohammed, C. Chen, Z. Zhu, *J. Colloid Interface Sci.* **538**, 308 (2019).
- [6] C. Young, T. Park, J. W. Yi, J. Kim, M. S. A. Hossain, Y. V. Kaneti, Y. Yamauchi, *ChemSusChem* **11**, 3546 (2018).
- [7] Y. Zhai, Y. Dou, D. Zhao, P. F. Fulvio, R. T. Mayes, S. Dai, *Adv. Mater.* **23**, 4828 (2011).
- [8] M. Danish, T. Ahmad, *Renew. Sustain. Energy Rev.* **87**, 1 (2018).
- [9] J. Lehmann, J. Gaunt, M. Rondon, *Mitig. Adapt. Strateg. Glob. Chang.* **11**, 403 (2006).
- [10] S. Rangabhashiyam, P. Balasubramanian, *Ind. Crops Prod.* **128**, 405 (2019).
- [11] L. Yan, J. Yu, J. Houston, N. Flores, H. Luo, *Green Energy Environ.* **2**, 84 (2017).
- [12] O. Fasakin, J. K. Dangbegnon, D. Y. Momodu, M. J. Madito, K. O. Oyedotun, M. A. Eleruja, N. Manyala, *Electrochim. Acta* **262**, 187 (2018).
- [13] E. Taer, Apriwandi, R. Taslim, Agustino, *Mater. Today Proc.*, 2021.
- [14] V. Yang, R. A. Senthil, J. Pan, A. Khan, S. Osman, L. Wang, W. Jiang, Y. Sun, *J. Electroanal. Chem.*, 113616 (2019).

- [15] J. Sodontipinta, T. Amornsakchai, P. Pakawatpanurut, *Adv. Nat. Sci. Nanosci. Nanotechnol.* **8**, 035017 (2017).
- [16] T. Ji, K. Han, Z. Teng, J. Li, M. Wang, J. Zhang, *Int. J. Electrochem. Sci.* **16**, 1 (2021).
- [17] C. K. Roy, S. S. Shah, A. H. Reaz, S. Sultana, A. N. Chowdhury, S. H. Firoz, M. H. Zahir, M. A. Ahmed Qasem, M. A. Aziz, *Chem. - An Asian J.* **16**, 296 (2021).
- [18] A. R. Selvaraj, A. Muthusamy, In-ho-Cho, H. J. Kim, K. Senthil, K. Prabakar, *Carbon N. Y.* **174**, 463 (2021).
- [19] Z. Xue, Q. Xiong, C. Zou, H. Chi, X. Hu, Z. Ji, *Mater. Res. Bull.* **133**, 111049 (2021).
- [20] Z. Shang, X. An, L. Liu, J. Yang, W. Zhang, H. Dai, H. Cao, Q. Xu, H. Liu, Y. Ni, *Carbohydr. Polym.* **251**, 117107 (2021).
- [21] J. Zhao, W. Han, M. Tu, S. Huan, R. Zeng, H. Wu, Z. Cha, C. Zhou, *Mater. Sci. Eng. C* **32**, 1496 (2012).
- [22] X. Liu, M. Naylor Marlow, S. J. Cooper, B. Song, X. Chen, N. P. Brandon, B. Wu, *J. Power Sources* **384**, 264 (2018).
- [23] W. Yang, Z. Shi, H. Guo, J. Guo, X. Lei, L. Yue, *Int. J. Electrochem. Sci.* **12**, 5587 (2017).
- [24] H. Wang, H. Niu, H. Wang, W. Wang, X. Jin, H. Wang, H. Zhou, T. Lin, *J. Power Sources* **482**, 228986 (2021).
- [25] K. Xu, S. Li, J. Yang, J. Hu, *J. Colloid Interface Sci.* **513**, 448 (2018).
- [26] Z. Lu, R. Raad, F. Safaei, J. Xi, Z. Liu, J. Foroughi, *Front. Mater.* **6**, 1 (2019).
- [27] E. Taer, L. Pratiwi, Apriwandi, W. S. Mustika, R. Taslim, Agustino, *Commun. Sci. Technol.* **5**, 22 (2020).
- [28] J. Serafin, M. Baca, M. Biegun, E. Mijowska, R. J. Kaleńczuk, J. Sreńscek-Nazzal, B. Michalkiewicz, *Appl. Surf. Sci.* **497**, 143722 (2019).
- [29] L. Liangshuo, Q. Lin, L. Xinyu, D. Ming, F. Xin, *Optoelectron. Adv. Mat.* **14**, 548 (2020).
- [30] T. Islam, M. M. Hasan, S. S. Shah, M. R. Karim, F. S. Al-Mubaddel, M. H. Zahir, M. A. Dar, M. D. Hossain, M. A. Aziz, A. J. S. Ahammad, *J. Energy Storage* **32**, 101908 (2020).
- [31] P. Thomas, C. W. Lai, M. R. Bin Johan, *J. Anal. Appl. Pyrolysis* **140**, 54 (2019).
- [32] Poonam, K. Sharma, A. Arora, S. K. Tripathi, *J. Energy Storage* **21**, 801 (2019).
- [33] A. González, E. Goikolea, J. A. Barrena, R. Mysyk, *Renew. Sustain. Energy Rev.* **58**, 1189 (2016).
- [34] S. Ahmed, M. Parvaz, R. Johari, M. Rafat, *Mater. Res. Express* **5**, 045601 (2018).
- [35] C. Saka, *J. Anal. Appl. Pyrolysis* **95**, 21 (2012).
- [36] E. R. K. Fernandes, C. Marangoni, O. Souza, N. Sellin, *Energy Convers. Manag.* **75**, 603 (2013).
- [37] Y. Boyjoo, Y. Cheng, H. Zhong, H. Tian, J. Pan, V. K. Pareek, S. P. Jiang, J. F. Lamonier, M. Jaroniec, J. Liu, *Carbon N. Y.* **116**, 490 (2017).
- [38] H. Chen, H. Wei, N. Fu, W. Qian, Y. Liu, H. Lin, S. Han, *J. Mater. Sci.* **53**, 2669 (2018).
- [39] P. Manasa, Z. J. Lei, F. Ran, *J. Energy Storage* **30**, 101494 (2020).
- [40] X. Liu, C. Ma, J. Li, B. Zielinska, R. J. Kalenczuk, X. Chen, P. K. Chu, T. Tang, E. Mijowska, *J. Power Sources* **412**, 1 (2019).
- [41] E. Taer, A. Apriwandi, R. Taslim, A. Agutino, D. A. Yusra, *J. Mater. Res. Technol.* **9**, 13332 (2020).
- [42] A. A. Hor, S. A. Hashmi, *Electrochim. Acta* **356**, 136826 (2020).
- [43] G. A. Yakaboylu, T. Yumak, C. Jiang, J. W. Zondlo, J. Wang, E. M. Sabolsky, *Energy and Fuels* **33**, 9309 (2019).
- [44] A. Gopalakrishnan, T. D. Raju, S. Badhulika, *Carbon N. Y.* **168**, 209 (2020).
- [45] E. Taer, Apriwandi, B. K. L. Dalimunthe, R. Taslim, *J. Chem. Technol. Biotechnol.* **96**, (2021).
- [46] A. Yaya, B. Agyei-Tuffour, D. Dodoo-Arhin, E. Nyankson, E. Annan, D. S. Konadu, E. Sinayobye, E. a. Baryeh, C. P. Ewels, *Glob. J. Eng. Des. Technol.* **1**, 32 (2012).
- [47] W. Jiang, J. Pan, X. Liu, *J. Power Sources* **409**, 13 (2019).
- [48] X. Ma, H. Wang, Q. Wu, J. Zhang, D. Liang, S. Lu, Y. Xiang, *J. Electrochem. Soc.* **166**, A236 (2019).
- [49] P. Cheng, T. Li, H. Yu, L. Zhi, Z. Liu, Z. Lei, *J. Phys. Chem. C* **120**, 2079 (2016).
- [50] V. Barranco, M. A. Lillo-Rodenas, A. Linares-Solano, A. Oya, F. Pico, J. Ibaññez,

- F. Agullo-Rueda, J. M. Amarilla, J. M. Rojo, *J. Phys. Chem. C* **114**, 10302 (2010).
- [51] F. Cheng, X. Yang, S. Zhang, W. Lu, *J. Power Sources* **450**, 227678 (2020).
- [52] E. Taer, A. Agustino, A. Awitdrus, R. Farma, R. Taslim, *J. Electrochem. Energy Convers. Storage* **18**, 1 (2020).
- [53] X. Hao, J. Wang, B. Ding, Y. Wang, Z. Chang, H. Dou, X. Zhang, *J. Power Sources* **352**, 34 (2017).
- [54] T. Wang, A. H. Rony, K. Sun, S. J. Smith, G. Eddings, M. Fan, T. Wang, A. H. Rony, K. Sun, W. Gong, X. He, W. Lu, M. Tang, *Cell Reports Phys. Sci.* **1**, 100079 (2020).
- [55] X. Q. Lin, N. Yang, L. Qiu-Feng, R. Liu, *Energy Technol.* **7**, (2019).
- [56] S. Ghosh, S. Barg, S. M. Jeong, K. Ostrikov, *Adv. Energy Mater.* **10**, 1 (2020).
- [57] X. L. Su, S. Jiang, G. P. Zheng, X. C. Zheng, J. H. Yang, Z. Y. Liu, *J. Mater. Sci.*, 1 (2018).
- [58] M. Deraman, N. S. M. Nor, E. Taer, B. Yatim, Awitdrus, R. Farma, N. H. Basri, M. A. R. Othman, R. Omar, M. R. M. Jasni, R. Daik, S. Soltaninejad, M. Suleman, G. Hegde, A. A. Astimar, *Mater. Sci. Forum* **846**, 497 (2016).
- [59] Q. Abbas, R. Raza, I. Shabbir, A. G. Olabi, *J. Sci. Adv. Mater. Devices* **4**, 341 (2019).
- [60] Y. Ma, X. Zhang, Z. Liang, C. Wang, Y. Sui, *Electrochim. Acta* **337**, 135800 (2020).
- [61] Y. P. Zhao, R. X. Xu, J. P. Cao, X. Y. Zhang, J. S. Zhu, X. Y. Wei, *J. Electroanal. Chem.* **871**, 114288 (2020).
- [62] S. Huo, X. Zhang, B. Liang, Y. Zhao, K. Li, *J. Power Sources* **450**, 227612 (2020).
- [63] M. K. Seo, S. J. Park, *Mater. Sci. Eng. B Solid-State Mater. Adv. Technol.* **164**, 106 (2009).
- [64] Z. Guo, X. Kong, X. Wu, W. Xing, J. Zhou, Y. Zhao, S. Zhuo, *Electrochim. Acta* **360**, 137022 (2020).
- [65] B. Chang, Y. Wang, K. Pei, S. Yang, X. Dong, *RSC Adv.* **4**, 40546 (2014).
- [66] E. E. Miller, Y. Hua, F. H. Tezel, *J. Energy Storage* **20**, 30 (2018).